Tunneling criteria and a nonadiabatic term for strong-field ionization

Hongcheng Ni,[1,*] Nicolas Eicke,[2] Camilo Ruiz,[3] Jun Cai,[4] Florian Oppermann,[2]
Nikolay I. Shvetsov-Shilovski,[2] and Liang-Wen Pi[1,†]

[1]*Max-Planck-Institut für Physik komplexer Systeme, Nöthnitzer Strasse 38, 01187 Dresden, Germany*
[2]*Institut für Theoretische Physik, Leibniz Universität Hannover, Appelstrasse 2, 30167 Hannover, Germany*
[3]*Instituto Universitario de Física Fundamental y Matemáticas y Departamento de Didáctica de la Matemática y de las Ciencias Experimentales, Universidad de Salamanca, Patio de las Escuelas s/n, 37008 Salamanca, Spain*
[4]*School of Physics and Electronic Engineering, Jiangsu Normal University, Xuzhou 221116, China*

(Received 30 May 2018; published 16 July 2018)

We investigate tunneling ionization of a model helium atom in a strong circularly polarized short laser pulse using the classical backpropagation method and compare ten different tunneling criteria on the same footing, aiming for a consistent classical picture of the tunneling dynamics. These tunneling criteria are categorized into velocity-based, position-based, and energy-based criteria according to different notions of a tunnel exit. We find that velocity-based criteria give consistent tunneling exit characteristics with nonadiabatic effects fully included. Other criteria are either inconsistent or only able to include nonadiabatic effects partially. Furthermore, we construct a simple tunneling rate formula, identify a term in the rate responsible for the nonadiabatic effects, and demonstrate the importance of this term.

DOI: 10.1103/PhysRevA.98.013411

I. INTRODUCTION

Tunneling ionization is fundamental to many strong-field phenomena as a common first step. A detailed description of its features is essential to understand and control related phenomena such as high-order harmonic generation [1–3] and many others. However, some basic properties of this process are still being debated, such as the position where the electron leaves the barrier and the time it takes for the electron to tunnel [4–6]. Advances in laser technology made it possible to assess these questions experimentally, for example, using the so-called attoclock technique. There, a strong elliptically polarized laser pulse ionizes a bound electron and subsequently deflects it to different directions depending on the time the electron is released, thereby mapping tunneling exit time to deflection angle [7,8]. This angle, however, can be modified by the interaction of the residual ion with the outgoing electron. Removing this Coulomb correction from the offset angle is unfortunately a nontrivial task, where theoretical support is always necessary and much of the discussion on the attoclock is rooted in the question of how exactly this has to be done.

In static or adiabatic tunneling in one spatial dimension, the commonly accepted classical picture of a barrier exit is when the total energy equals the potential energy, or when the kinetic energy is zero, which we call the zero-kinetic-energy principle hereafter. Since the total energy is conserved, the tunnel exit can be determined unambiguously. In reality, tunneling ionization occurs in a time-dependent field, where constant tunneling energy during under-barrier motion cannot be assumed [9–11]. This assumption, nevertheless, has been commonly made to obtain the Coulomb correction [12] with classical-trajectory-based methods [13–15] starting from certain predefined tunneling exit positions given by the static (or Stark-shifted) ionization potential. In addition, instantaneous tunneling is also assumed to launch the trajectory, which contradicts any tunneling time delay found in the end. Moreover, in more than one spatial dimension ambiguities arise in the choice of the tunneling coordinate.

Classical backpropagation [16,17] avoids these problems by treating the ionization step fully quantum mechanically. The ionized wave packet is transformed into classical trajectories via the local-momentum method [18–20] and propagated backwards in time to retrieve the tunneling exit information. By choosing different criteria to stop these backpropagating trajectories, we compared different assumptions and approximations to the tunneling dynamics on the same footing and found [17] that the discrepancies in the literature regarding tunneling time delay [12,16,21–27] depend on the degree to which nonadiabaticity is taken into account and plays a role.

As commonly used, the position criterion considers an electron to tunnel out at a certain position given by the static ionization potential and thus neglects any change in exit position due to nonadiabatic energy variation across the barrier. It results in a positive tunneling time delay and nonvanishing longitudinal tunneling velocity [24,25]. In contrast, the velocity criterion, which is a straightforward extrapolation of the zero-kinetic-energy principle to higher dimensions, considers an electron to tunnel out with vanishing longitudinal velocity (vanishing velocity in the instantaneous field direction). It fully accounts for nonadiabaticity and results in zero tunneling time delay [16,17]. In this article, we study eight more tunneling criteria that are physically intuitive. These criteria can be categorized into velocity-based criteria (e.g., the velocity

*Institute of Theoretical Physics, Technische Universität Wien, Wiedner Hauptstrasse 8-10/136, 1040 Vienna, Austria.
†lwpi@pks.mpg.de

criterion), position-based criteria (e.g., the position criterion), and energy-based criteria.

Formally, all tunneling criteria are equivalently suitable as a classical picture of the quantum tunneling process, as long as the ionizing wave packet is composed of trajectories that actually start at some point according to the criterion in question. In other words, some of these criteria may not be suitable due to their failure to account for the observed tunneling probability because some backpropagated trajectories might never fulfill the respective tunneling criterion. This can be quantified using the nontunneled fraction [16,17]. Here, we show that the velocity-based criteria are suitable candidates in the sense above for the classical picture of the quantum tunneling dynamics. These criteria are consistent generalizations to the principle of zero kinetic energy, which defines the tunneling barrier, while other criteria are not (in the case of nonadiabatic tunneling ionization).

Furthermore, a study using the adiabatic expansion [28–31] of strong-field approximation (SFA) reveals that nonadiabaticity can be accounted for accurately with a simple tunneling formula similar to the Ammosov-Delone-Krainov (ADK) theory [32–34] but with a different denominator in the exponent. We stress the importance of this term and demonstrate its effects on the tunneling exit characteristics.

The article is organized as follows. In Sec. II we briefly describe the classical backpropagation method and different tunneling criteria. In Sec. III we compare the tunneling exit characteristics given by different tunneling criteria. In Sec. IV we study the tunneling exit characteristics given by SFA and identify the nonadiabatic term for tunneling ionization. In Sec. V we study the suitability of different criteria using the nontunneled fraction. Conclusions are given in Sec. VI. Atomic units are used throughout unless stated otherwise.

II. CLASSICAL BACKPROPAGATION AND TUNNELING CRITERIA

The essence of the classical backpropagation method is a quantum forward propagation followed by a classical backpropagation.

A. Quantum forward propagation

The quantum forward propagation treats the tunneling dynamics fully quantum-mechanically. As before [16,17], the forward propagation is done by solving the time-dependent Schrödinger equation (TDSE) using the split-step Fourier method for a two-dimensional model helium atom with a single active electron. The potential is adopted from Ref. [35] but with the radius r replaced by a soft core $\sqrt{r^2+a}$, where a is tuned to obtain the ionization potential $I_p = 0.904$ of helium. The laser field $\boldsymbol{F}(t) = -\frac{d}{dt}\boldsymbol{A}(t)$ is derived from the vector potential

$$\boldsymbol{A}(t) = \frac{A_0}{\sqrt{2}}\cos^4\left(\frac{\omega t}{4}\right)\begin{pmatrix}\cos(\omega t)\\ \sin(\omega t)\end{pmatrix}, \tag{1}$$

representing a two-cycle circularly polarized laser pulse centered at $t = 0$ with $\omega = 0.045$ corresponding to 1000-nm wavelength. The peak intensity is varied from 2.0×10^{14} to 8.0×10^{14} W/cm^2.

B. Classical backpropagation

The resulting quantum ionized wave packet $\psi(\boldsymbol{r},t')$ is transformed into classical trajectories at each grid point $\boldsymbol{r}$. The momentum of the classical trajectory at $\boldsymbol{r}$ is obtained by the local-momentum method [18–20],

$$\boldsymbol{k}(\boldsymbol{r},t') = \nabla S(\boldsymbol{r},t'), \tag{2}$$

where $S(\boldsymbol{r},t') \equiv \arg\{\psi(\boldsymbol{r},t')\}$, and the weight of the classical trajectory is $|\psi(\boldsymbol{r},t')|^2$. The classical trajectories are then backpropagated until reaching the tunneling barrier, which is defined by the tunneling criteria below.

C. Tunneling criteria

For each trajectory, the backpropagation is stopped when the tunneling criterion is met. The criteria themselves are based on physical intuition and different classical perspectives of the tunneling process. All criteria considered here are time dependent. They can be categorized into three groups: velocity-based, position-based, and energy-based criteria. In case multiple solutions to a tunneling criterion exist, we take the one closest to the core as the true tunnel exit [16,17], while for position-based criteria, the solution with lowest speed is taken.

1. Velocity criterion

Let us start from the one-dimensional tunneling scenario. Here, the tunnel exit sits where the kinetic energy or the velocity is zero. In a rotating laser field, it is intuitive to set the velocity in the instantaneous field direction $\hat{\boldsymbol{F}}$ to zero, i.e., in the direction tunneling optimally occurs. The velocity criterion thus reads

$$k_\parallel \equiv -\boldsymbol{k}\cdot\hat{\boldsymbol{F}} = 0. \tag{3a}$$

In fact, this criterion can be derived from the seminal Keldysh theory [36,37], according to which for a long circularly polarized laser pulse the velocity component in the direction of the laser field must vanish at the tunnel exit, i.e., the time that corresponds to the real part of the complex ionization time [28–31]. For arbitrary field shapes this statement is still true in the tunneling limit, i.e., when expanding the saddle-point equation up to second order in the Keldysh parameter.

2. Parabolic velocity criterion

The static tunneling ionization process is a separable problem in parabolic coordinates [38] defined by the (instantaneous) electric field in which tunneling is only possible through the η coordinate, where $\eta = r - \hat{\boldsymbol{F}}\cdot\boldsymbol{r}$. Following along the lines of the velocity criterion, one may postulate a vanishing velocity in the η coordinate:

$$k_\eta \equiv \frac{d}{dt}(r - \hat{\boldsymbol{F}}\cdot\boldsymbol{r}) = 0. \tag{3b}$$

3. Turning point criterion

The tunnel exit in the one-dimensional case corresponds to the classical turning point of the incident particle and can be intuitively extended to higher-dimensional systems, where the

turning point criterion reads

$$k_r \equiv \boldsymbol{k} \cdot \hat{\boldsymbol{r}} = 0. \tag{3c}$$

The turning point criterion gives a tunneling exit position as close as possible to the core during the backpropagation of a trajectory. It is related to the above criteria in the sense that the (parabolic) velocity criterion becomes the turning point criterion assuming $-\boldsymbol{F} \parallel \boldsymbol{r}$, which is roughly met.

4. Minimal speed criterion

The zero-kinetic-energy principle also indicates a local minimum in the speed of the particle,

$$\dot{k} \equiv \frac{d}{dt}|\boldsymbol{k}| = 0, \quad (\ddot{k} > 0), \tag{3d}$$

which is another possible generalization of the one-dimensional tunneling picture to higher dimensions. We note that $\frac{d}{dt}|\boldsymbol{k}| \neq |\frac{d}{dt}\boldsymbol{k}|$.

The velocity, parabolic velocity, turning point, and minimal speed criteria all hinge on the velocity and we group them as velocity-based criteria. None of them assume static tunneling energy and thus they account fully for nonadiabatic effects. These criteria are consistent generalizations to the zero-kinetic-energy principle, even in the case of nonadiabatic tunneling ionization.

5. Position criterion

In the static tunneling scenario, zero kinetic energy occurs at the position where the static total energy matches the potential energy. During tunneling ionization in a varying laser field, the total energy is generally not conserved. Nevertheless, constant tunneling energy is commonly assumed, and the position criterion here considers an electron to tunnel out at certain positions given by the static ionization potential I_p. It has been widely used to launch (forward-propagating) classical trajectories to find the Coulomb correction in the attoclock setup. There are also different definitions of the position where an electron should tunnel out, but here we restrict ourselves to the tunneling exit position given in parabolic coordinates [38], as other definitions give qualitatively similar results regarding tunneling time delay and other tunneling exit characteristics [17]. The position criterion can be written as [39]

$$r = \frac{I_p + \sqrt{I_p^2 - 4\beta F}}{2F}, \tag{3e}$$

where $\beta = 1 - \sqrt{2I_p}/2$ for the three-dimensional case [38]. For a two-dimensional system, the separation constant β is in principle different. Following the recipe in Ref. [38], we find $\beta_{2D} = 1 - \sqrt{2I_p}/4$ for the two-dimensional ground state. However, the resulting tunneling exit coordinates do not have any qualitative difference compared to those obtained using the three-dimensional separation constant. Thus, we stick to the commonly used three-dimensional separation constant in this study. The reader is referred to the Appendix for a study of different variants of the position criterion.

6. Stark position criterion

The Stark position criterion considers an electron to tunnel out at certain positions given by the Stark-shifted ionization potential I_p^{Stark},

$$r = \frac{I_p^{\text{Stark}} + \sqrt{\left(I_p^{\text{Stark}}\right)^2 - 4\beta^{\text{Stark}} F}}{2F}, \tag{3f}$$

where $\beta^{\text{Stark}} = 1 - \sqrt{2I_p^{\text{Stark}}}/2$, $I_p^{\text{Stark}} = I_p + \frac{1}{2}\alpha F^2$, and $\alpha = 1.57$ is the polarizability of the two-dimensional model helium atom, which is obtained numerically by observing the energy change due to a range of small external static electric fields. This criterion, based on the "TIPIS" model [21], accounts for the position variations due to Stark shift of the initial state but not for nonadiabatic energy changes under the barrier.

7. Dynamic position criterion

The dynamic position criterion considers an electron to tunnel out at certain positions given by its instantaneous binding energy $-E$,

$$r = \frac{-E + \sqrt{E^2 - 4\beta^{\text{inst}} F}}{2F}, \tag{3g}$$

where $\beta^{\text{inst}} = 1 - \sqrt{-2E}/2$. Although the (Stark) position criterion assumes constant tunneling energy through the barrier to obtain the tunneling exit position, the energy we find at the exit position is indeed different than assumed [17], which will become clear later. The dynamic position criterion resolves this inconsistency by determining the tunneling exit position on the fly based on the instantaneous energy of the electron.

The position, Stark position, and dynamic position criteria are based on the position of the electron and we categorize them as position-based criteria. Both velocity-based and position-based criteria root from the zero-kinetic-energy principle, but position-based criteria additionally assume static total energy for under-barrier motion, which leads to difficulties and inconsistencies, as we will show later.

8. Static energy criterion

The static energy criterion considers an electron to tunnel through the barrier with constant ground-state energy

$$E = -I_p. \tag{3h}$$

It neglects any energy variation of the initial state and during the under-barrier motion. In contrast to the position criterion, which determines the tunneling exit position from the constant total energy, the static energy criterion assesses the total energy directly.

9. Stark energy criterion

The Stark energy criterion considers an electron to tunnel through the barrier with constant Stark-shifted ground-state energy

$$E = -I_p^{\text{Stark}}. \tag{3i}$$

This criterion takes into account the Stark shift of the initial state but neglects nonadiabatic energy variation across the barrier.

The static energy and Stark energy criteria are based on the total energy and thus we group them as (total-)energy-based criteria. It should be noted that energy-based criteria are questionable as tunneling criteria to begin with. In a static tunneling process, the total energy is conserved, hence these energy-based criteria would be fulfilled everywhere on a backpropagating trajectory and cannot give any meaningful tunneling exit information. On the other hand, in tunneling ionization where energy variation is present, these criteria are fulfilled almost nowhere for most backpropagating trajectories, as we will show later.

D. Nontunneled fraction

To quantify the suitability of different criteria as a classical picture of the tunneling dynamics, we collect the fraction of trajectories that never meet the tunneling criterion during the course of backpropagation [16,17],

$$\chi = \frac{P_{\rm ion} - P_{\rm tun}}{P_{\rm ion}}, \tag{4}$$

where $P_{\rm ion}$ is the ionization probability at the end of the quantum forward propagation and $P_{\rm tun}$ is the fraction of trajectories that meets the respective tunneling criterion. For the nontunneled fraction of ionization probability, no matter what combination of initial tunneling exit conditions is used, the accurate asymptotics cannot be reproduced. The nontunneled fraction χ denotes to what degree the ionization can be considered as tunneling according to each tunneling criterion. It should be sufficiently low in the tunneling regime, and thus can be used as a quantification of the suitability of different tunneling criteria.

III. TUNNELING EXIT CHARACTERISTICS FROM DIFFERENT TUNNELING CRITERIA

In this section, we study the tunneling exit characteristics given by different stopping criteria using classical backpropagation, which gives highly correlated information regarding the tunneling exit. In the most differential setting, it gives a correlated distribution of tunneling exit position (x and y), tunneling exit time τ, longitudinal tunneling momentum $k_\parallel$, and transverse tunneling momentum $k_\perp$. The tunneling energy E (total energy at the tunnel exit) can also be obtained from this correlated distribution. The results are summarized in Fig. 1 for a peak intensity of 8×10^{14} W/cm^2, projected onto different exit coordinates.

A. Velocity criterion

Figure 1(a) shows the tunneling exit characteristics obtained using the velocity criterion. As shown before [16,17], the velocity criterion fully incorporates nonadiabatic tunneling effects. This is achieved by introducing a broad distribution of tunneling exit points as shown in Fig. 1(a1), in contrast to introducing a nonzero longitudinal tunneling momentum for a fixed tunneling exit point [24,25,40–44]. The latter, however, leads to inconsistencies and difficulties, as we will show later in Secs. III E–III G.

With the velocity criterion, a zero tunneling time delay results, as is clear from Fig. 1(a2). There, the distribution of tunneling exit time τ is close to a Gaussian distribution centered nearly at zero.

The longitudinal tunneling momentum $k_\parallel$ (velocity in the instantaneous field direction), by definition of the velocity tunneling criterion, is zero, as shown in Fig. 1(a3). In contrast, there is a nonzero shift in the transverse tunneling momentum $k_\perp$ (velocity perpendicular to the instantaneous field direction) with Gaussian spreading [Fig. 1(a4)], in agreement with the Perelomov-Popov-Terent'ev (PPT) theory [45–50], as shown before [17].

Figure 1(a5) shows the energy distribution at the tunnel exit. Obviously, an electron may gain or lose energy during its motion towards the exit. For those electrons that lose energy, they end up with a large tunneling exit distance to the core and form the far-out part of the tunneling exit point distribution in Fig. 1(a1), while for those electrons that gain energy, they tunnel out at a closer distance to the parent ion.

It is also instructive to study the dependence of the tunneling energy on exit time, as shown in Fig. 2. Integration of such distribution over the energy axis gives Fig. 1(a2), and integration of it over the time axis gives Fig. 1(a5). It can be seen that the energy absorption is preferred to energy loss at all times during the laser pulse. At the leading and trailing edges of the laser pulse, when the laser intensity is comparatively low, tunneling electrons absorb more energy than near the peak intensity. This is because the tunneling barrier is thicker at both edges and the electron has more chance to absorb energy from the laser field. The nonadiabatic energy gain can also be interpreted as a virtual absorption of photons, or polarization of the initial state, followed by a static tunneling ionization [51], where it is shown that more photons are virtually absorbed as the laser intensity decreases.

B. Parabolic velocity criterion

The instantaneous laser electric field direction defines both a Cartesian and a parabolic coordinate. Instead of using zero velocity in the Cartesian tunneling coordinate, as it is the case for the velocity criterion (3a), we can also apply a vanishing velocity in the parabolic tunneling coordinate, leading to the parabolic velocity criterion (3b). The corresponding tunneling exit information is shown in Fig. 1(b), which is very similar to (indeed almost the same as) Fig. 1(a). For a pure tunneling process, the kinetic energy at the tunnel exit is very small. It is thus natural that the velocity and parabolic velocity criteria give similar results, although they require zero kinetic energy in different coordinates. Their similarity can be seen from a typical backpropagating trajectory in Fig. 3, where it is clear that the points identified by both criteria are very close to each other. In addition, the parabolic velocity criterion gives a nonzero longitudinal tunneling momentum as shown in Fig. 1(b3), which is a very narrow peak located at zero, which is also an indication of the similarity of tunneling exit results given by both criteria.

C. Turning point criterion

The turning point criterion (3c) considers an electron to tunnel out at the classical turning point. In the tunneling regime, the exit point $\boldsymbol{r}$ follows closely the field direction $\hat{\boldsymbol{F}}$ [16]. The

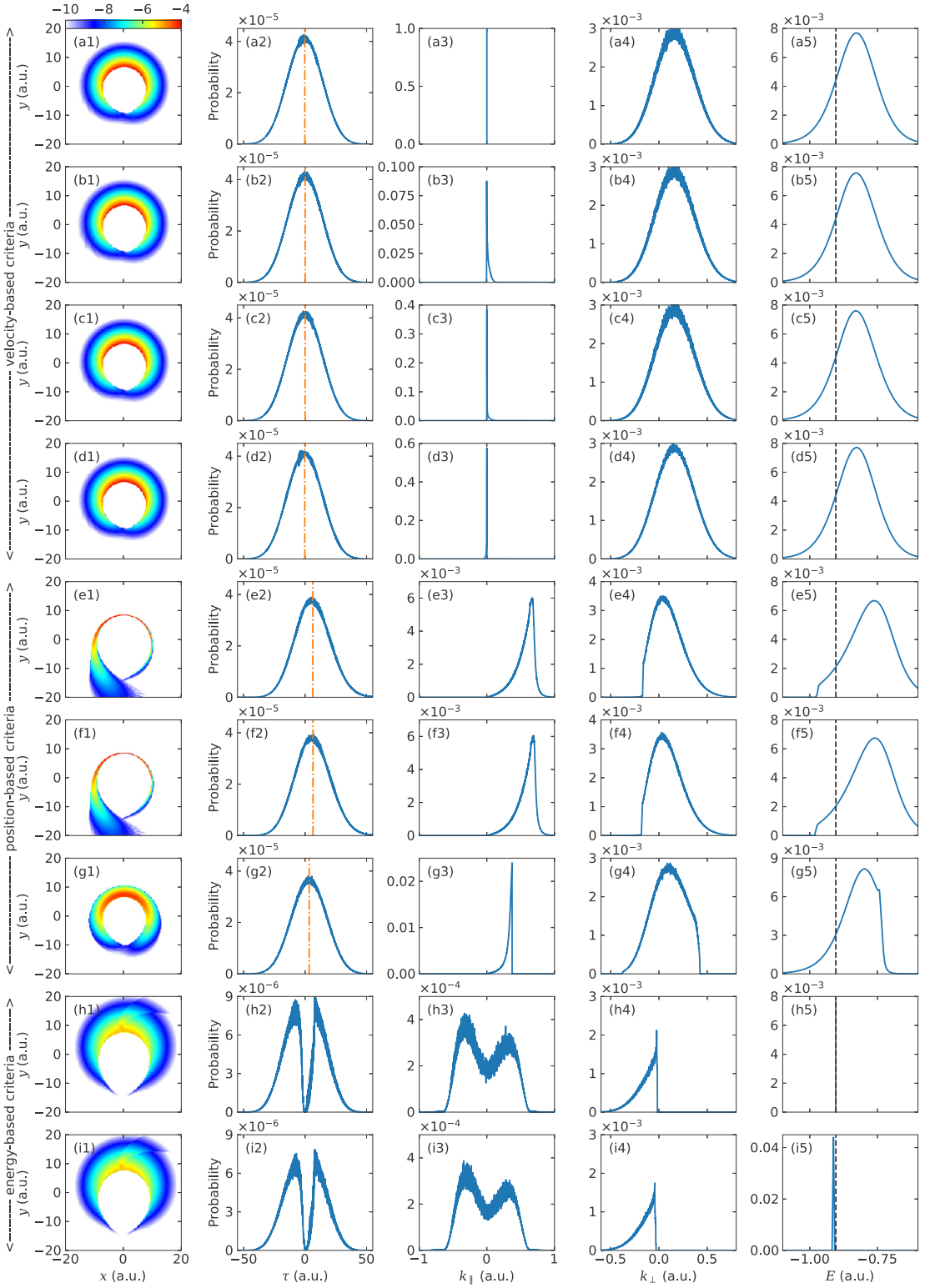

FIG. 1. Tunneling exit characteristics of the model helium atom obtained by different tunneling criteria in a laser field with peak intensity 8×10^{14} W/cm^2. Other laser parameters are given in the text. By row: (a) velocity criterion (3a); (b) parabolic velocity criterion (3b); (c) turning point criterion (3c); (d) minimal speed criterion (3d); (e) position criterion (3e); (f) Stark position criterion (3f); (g) dynamic position criterion (3g); (h) static energy criterion (3h); (i) Stark energy criterion (3i). By column: (1) distribution of tunneling exit position in x-y plane (in logarithmic scale); (2) distribution of tunneling exit time τ, where orange dash-dotted lines denote the expected time (not shown for energy-based criteria); (3) distribution of longitudinal tunneling momentum $k_\parallel$; (4) distribution of transverse tunneling momentum $k_\perp$; (5) distribution of tunneling energy E, where black dashed lines denote the ground-state energy $-I_p$.

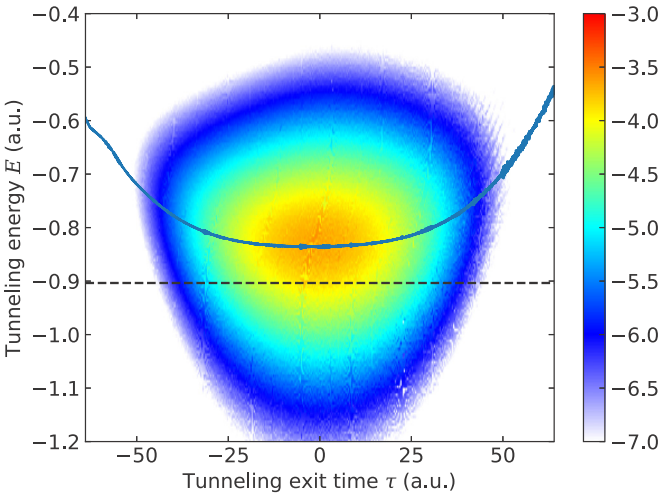

FIG. 2. Correlated distribution of tunneling energy E and tunneling exit time τ (in logarithmic scale) of the model helium atom obtained by the velocity tunneling criterion. The blue solid line denotes the expected tunneling energy at different tunneling exit times, and the black dashed line denotes the ground-state energy $-I_p$. Laser parameters are the same as in Fig. 1.

turning point criterion (3c) thus is expected to give tunneling exit coordinates very close to that of the velocity (3a) and parabolic velocity criteria (3b). This is indeed what we find comparing Fig. 1(c) to Figs. 1(a) and 1(b) and also from Fig. 3.

D. Minimal speed criterion

The minimal speed criterion keeps track of the speed of the electron during backpropagation and considers it to tunnel out at a local minimum of its speed (3d), which gives a tunnel exit

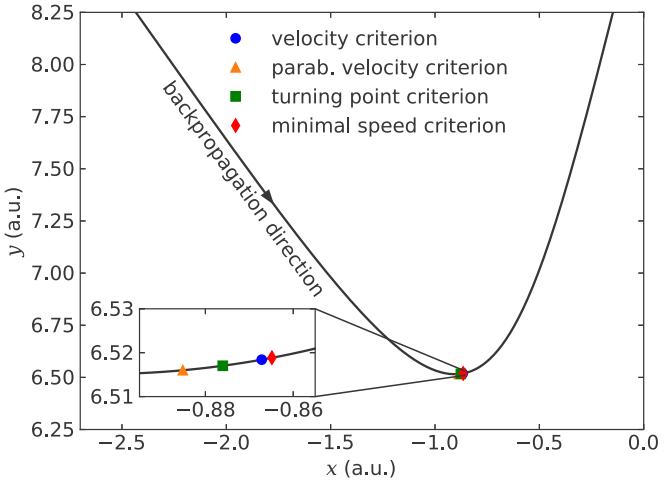

FIG. 3. The central part of a typical backpropagating trajectory from the ionized wave packet of the model helium atom. The blue filled circle denotes the exit point in the velocity criterion, the orange triangle denotes the exit point in the parabolic velocity criterion, the green square denotes the exit point in the turning point criterion, and the red diamond denotes the exit point in the minimal speed criterion. A zoom-in near the exit points is provided in the inset. Laser parameters are the same as in Fig. 1.

TABLE I. Similarity among velocity-based criteria. Laser parameters are the same as in Fig. 1.

Tunneling criterion	$\langle k_\parallel \rangle$	$\langle k_\eta \rangle$	$\langle k_r \rangle$	$\langle \dot{k} \rangle$
Velocity	0	−0.0475	−0.0222	0.0016
Parabolic velocity	0.0240	0	0.0018	0.0088
Turning point	0.0219	−0.0034	0	0.0070
Minimal speed	−0.0063	−0.0619	−0.0285	0
Position	0.5620	0.9881	0.5332	0.0845

close to that of (parabolic) velocity and turning point criteria, as can be seen in Fig. 3. Similarly, tunneling exit characteristics in Fig. 1(d) are close to those of other velocity-based criteria [Figs. 1(a)–1(c)].

The similarity of the tunneling exit characteristics given by the velocity-based criteria (velocity, parabolic velocity, turning point, and minimal speed criteria) is rooted in the fact that they all stem from the zero-kinetic-energy principle, generalized to higher dimensions in different ways. The similarity can be quantified by studying their respective expected characteristic variables (the per-criterion vanishing variable) under different criteria, as shown in Table I. Apparently, all values from velocity-based criteria are very close to zero, indicating close resemblance among them. For comparison, we also include the values under the position criterion, which obviously deviate from zero.

E. Position criterion

The position criterion (3e) considers an electron to tunnel out at the position given by the static ground-state ionization potential, which thus is a thin line around the core as shown in Fig. 1(e1). Due to the quantum spreading of the ionizing wave packet, the position criterion specifies the tunneling distance but not the tunneling angle. Correspondingly, the distribution of the tunneling exit position is not strictly a line but has a width. The width of the distribution is minimal near the pulse center, indicating a more adiabatic scenario, or a more close concentration of the tunneling exit position near the direction of the laser field vector.

With this position criterion, a shift of the tunneling exit time to the positive direction, or a positive tunneling time delay [24,25], is observed, as shown in Fig. 1(e2). This can be understood as follows. Taking the tunneling exit position given by the velocity criterion [Fig. 1(a1)] as the reference that leads to zero tunneling time delay and noting that it has an average distance to the core smaller than that of the position criterion [Fig. 1(e1)] due to nonadiabatic energy absorption, the time the electron takes to propagate from the reference position to the position specified in the position criterion would show up in the tunneling exit time here, resulting in a positive tunneling time delay. Along the same line, a positive longitudinal tunneling momentum is found, as shown in Fig. 1(e3), since the electron is accelerated outwards from the reference position, which has zero longitudinal tunneling momentum.

The transverse tunneling momentum [Fig. 1(e4)], however, has some unexpected features. It is essentially a Gaussian distribution but with a sharp cutoff at one side. Indeed, the

cut-off part corresponds to the low-energy part, as evident from Fig. 1(e5), which in turn corresponds to a tunneling exit position far out from the core [cf., Fig. 1(a1)]. However, these parts of the tunneling exit point are not covered by the position criterion, since the corresponding backpropagating trajectories can never reach the distance specified in the position criterion before they turn away from the core. That is to say, the position criterion cannot describe those tunneling electrons that have low energy and far-out tunneling exit position, which is also reflected in a high nontunneled fraction ($\chi = 0.0725$).

In addition to this problem, the tunneling energy obtained in the position criterion is actually different from the static ground-state energy, as shown in Fig. 1(e5). To obtain the tunneling exit position (3e), however, a static tunneling energy equal to $-I_p$ is assumed, which leads to inconsistency.

The reader is referred to the Appendix for a further study of different variants of the position criterion.

F. Stark position criterion

With these problems in mind, one may try a different version of the position criterion, where the Stark shift of the initial state is included (3f). This leads to a tunneling exit distance slightly farther away from the core than in the position criterion, as apparent from a comparison of Figs. 1(f1) to 1(e1). This enlarged tunneling distance slightly improves the capability of the Stark position criterion to cover more ionization probability ($\chi = 0.0657$). This can also be seen from Figs. 1(f4) and 1(f5), where the cut-off parts are smaller. The resulting distributions of tunneling exit time [Fig. 1(f2)] and longitudinal tunneling momentum [Fig. 1(f3)] are also similar to those of the position criterion (with small shifts and reshapes). We note that the inconsistency between the criterion and its underlying assumption of static tunneling energy $-I_p^{\text{Stark}}$ is still present.

G. Dynamic position criterion

To remove the inconsistency above, we keep track of the instantaneous energy of the electron while backpropagating and determine the tunneling exit position on the fly (3g). The resulting distributions of tunneling exit position [Fig. 1(g1)], time [Fig. 1(g2)], and longitudinal momentum [Fig. 1(g3)] are actually somewhere between those from the velocity-based criteria and the (Stark) position criterion.

However, the cutoff in the transverse tunneling momentum is still present at the positive side [Fig. 1(g4)], which corresponds to the high-energy part [Fig. 1(g5)]. Higher energy leads to a decrease in the tunneling exit distance in the dynamic position criterion, and thus less ionization probability is covered there. In addition, the nontunneled fraction here is still high ($\chi = 0.118$).

H. Static energy criterion

The static energy criterion (3h) assumes the electron tunnels out with static ground-state energy. Compared to the velocity-based criteria where energy is preferentially absorbed, the static energy criterion leads to a distribution of tunneling exit points farther out, which is obvious from a comparison of Figs. 1(h1) to 1(a1). Given our previous concerns about the suitability of energy-based criteria and the fact that nonadiabaticity is completely neglected, it is not surprising that the tunneling exit characteristics show some strange features. Near the top of Fig. 1(h1), which corresponds to ionization around the pulse center, the exit point is pushed even farther out than nearby regions. Nonintuitive features also show up in the tunneling exit time in Fig. 1(h2), where a dip at pulse center is found. For the longitudinal tunneling momentum in Fig. 1(h3), there is also a dip around zero, and for the transverse tunneling momentum in Fig. 1(h4), an abrupt cutoff is present. The tunneling energy, on the other hand, is simply $-I_p$ by definition, as shown in Fig. 1(h5).

One should especially pay attention to the different scale in Fig. 1(h) as compared to Fig. 1(a). The substantially decreased ionization probability using the static energy criterion points to a very high nontunneled fraction ($\chi = 0.809$), meaning that the static energy criterion cannot cover the majority of the ionization probability. This simply tells us that the present criterion fails completely. In contrast to static tunneling where the static energy criterion is fulfilled everywhere, it is fulfilled almost nowhere in the case of nonadiabatic tunneling ionization.

I. Stark energy criterion

Given the failure of the static energy criterion, one may wonder if the Stark energy criterion (3i) is a remedy. As shown in Fig. 1(i), the same problems persist. To make things even worse, the ionization probability covered by this criterion is even lower ($\chi = 0.834$). This is indeed easy to understand. As shown in Figs. 1(a5) and 2, energy is preferentially gained during the tunneling ionization; the Stark-shifted energy, however, is even lower than the ground-state energy $-I_p$, making this criterion even harder to cover the corresponding ionization yield.

IV. TUNNELING EXIT CHARACTERISTICS FROM STRONG-FIELD APPROXIMATION

Many of the above tunneling exit characteristics obtained by classical backpropagation can indeed be qualitatively reproduced by SFA. In SFA, one solves the saddle-point equation

$$\tfrac{1}{2}[\boldsymbol{p} + \boldsymbol{A}(t_s)]^2 + I_p = 0, \tag{5}$$

where $\boldsymbol{p}$ is the conserved asymptotic momentum, and the saddle-point time $t_s = \tau + it_i$ must be complex to satisfy this equation. Here, τ is the tunneling exit time (or "ionization time") and t_i is sometimes called "tunneling time," which is related to the ionization rate and should be distinguished from the tunneling exit time τ. The (modified) SFA transition rate can be determined by [52–54]

$$W_{\text{SFA}} \approx \frac{\exp(2\text{Im}S)}{|[\boldsymbol{p} + \boldsymbol{A}(t_s)] \cdot \boldsymbol{F}(t_s)|^{1+Z/\sqrt{2I_p}}}, \tag{6}$$

with $Z = 1$ representing the parent ion charge and

$$S = \int_{t_s}^{\tau} \left\{ \frac{1}{2}[\boldsymbol{p} + \boldsymbol{A}(t)]^2 + I_p \right\} dt. \tag{7}$$

The tunneling exit position can be obtained by

$$\boldsymbol{r}_{\mathrm{SFA}} = \mathrm{Re}\int_{t_s}^{\tau}[\boldsymbol{p}+\boldsymbol{A}(t)]dt = \mathrm{Im}\int_{0}^{t_i}\boldsymbol{A}(\tau+it)dt. \quad (8)$$

In Fig. 4(a), we show the tunneling exit characteristics obtained by the above SFA calculations. For comparison, the results from classical backpropagation using the velocity criterion is plotted on top as orange dash-dotted lines (except tunneling exit position distribution). The SFA results are scaled in magnitude to match those of backpropagation. One can clearly see that the results from SFA and backpropagation agree very well. The SFA energy is slightly higher than that of backpropagation. This is expected because of the neglect of Coulomb potential energy. Since SFA does not restrict the longitudinal tunneling momentum $k_\parallel$, it shows up as a narrow peak at zero [55,56]. (This is due to the pulse envelope in the current situation. See also Ref. [17] for a comparison to PPT theory [45–50], which does not take the pulse envelope into account.)

A simplification of the SFA calculation close to the adiabatic case [28–31] is indeed plausible. The adiabatic expansion of the SFA formalism in powers of the Keldysh parameter often provides sufficient accuracy for nonadiabatic tunneling, even if only a few terms are retained, which also greatly facilitates calculations. A recent application of such expansion includes the Coulomb factor for the photoelectron spectrum [31], which was shown to largely improve the photoelectron momentum distribution with respect to the well-known static-field Coulomb factor [47]. To do this, we may expand the vector potential in terms of small t_i (or small Keldysh parameter γ corresponding to a tunneling scenario),

$$\boldsymbol{A}(\tau+it_i) = \boldsymbol{A}(\tau) - it_i\boldsymbol{F}(\tau) + \tfrac{1}{2}t_i^2\boldsymbol{F}'(\tau) + O\left(t_i^3\right), \quad (9)$$

where $\boldsymbol{F}'(\tau) = \frac{d\boldsymbol{F}(\tau)}{d\tau}$. Inserting the above expansion into Eq. (5) and keeping the terms up to the second order in t_i results in

$$\boldsymbol{k}(\tau)\cdot\boldsymbol{F}(\tau) = 0, \quad (10)$$

which is the velocity criterion (3a), and

$$t_i = \sqrt{\frac{k^2(\tau)+2I_p}{F^2(\tau)-\boldsymbol{k}(\tau)\cdot\boldsymbol{F}'(\tau)}}, \quad (11)$$

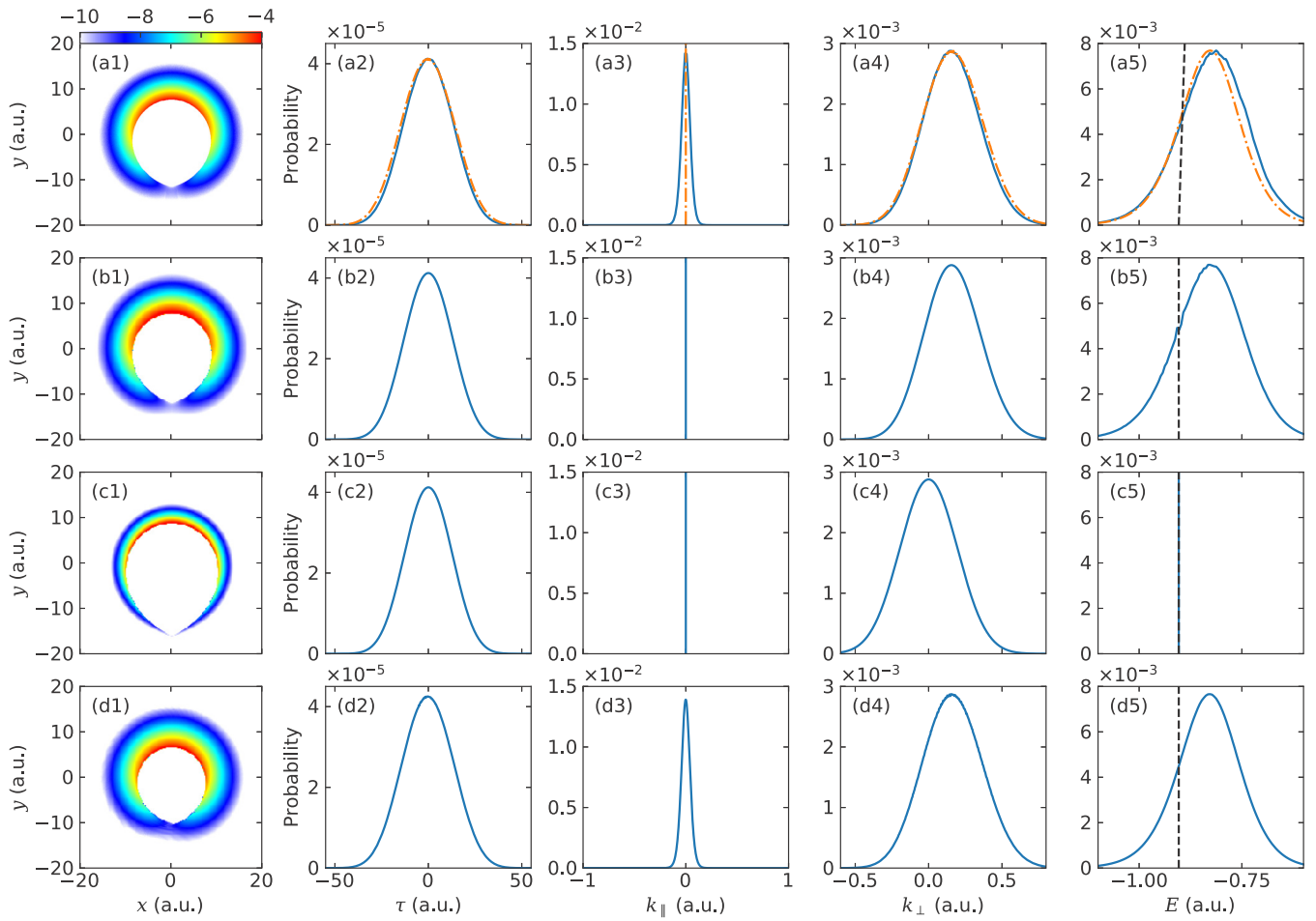

FIG. 4. Tunneling exit characteristics of the model helium atom obtained by different methods. By row: (a) SFA (for comparison, results of classical backpropagation using the velocity criterion are plotted as orange dash-dotted lines); (b) adiabatic expansion of SFA; (c) ADK theory; (d) classical backpropagation using elliptical velocity criterion. By column: (1) distribution of tunneling exit position in x-y plane (in logarithmic scale); (2) distribution of tunneling exit time τ; (3) distribution of longitudinal tunneling momentum $k_\parallel$; (4) distribution of transverse tunneling momentum $k_\perp$; (5) distribution of tunneling energy E, where black dashed lines denote the ground-state energy $-I_p$. Laser parameters are the same as in Fig. 1.

where $\boldsymbol{k}(\tau) = \boldsymbol{p} + \boldsymbol{A}(\tau)$. The ionization rate (6) can be calculated with

$$\begin{aligned} \mathrm{Im}S &= -I_p t_i - \frac{1}{2}\mathrm{Re}\int_0^{t_i} [\boldsymbol{p} + \boldsymbol{A}(\tau + it)]^2 dt \\ &\approx -I_p t_i - \frac{1}{2}\mathrm{Re}\int_0^{t_i} \left[\boldsymbol{k}(\tau) - it\boldsymbol{F}(\tau) + \frac{1}{2}t^2\boldsymbol{F}'(\tau)\right]^2 dt \\ &\approx -\frac{[k^2(\tau) + 2I_p]^{3/2}}{3\sqrt{F^2(\tau) - \boldsymbol{k}(\tau)\cdot\boldsymbol{F}'(\tau)}}, \end{aligned} \tag{12}$$

leading to (up to exponential accuracy) [31]

$$W_{\text{SFA-AE}}(\boldsymbol{k}_\perp, \boldsymbol{F}) \approx \exp\left[-\frac{2(k_\perp^2 + 2I_p)^{3/2}}{3\sqrt{F^2 - \boldsymbol{k}_\perp\cdot\boldsymbol{F}'}}\right], \tag{13}$$

where the transverse velocity at the tunnel exit, $\boldsymbol{k}_\perp$, is equivalent to $\boldsymbol{k}(\tau)$ within the current second-order expansion on t_i. The dependence on τ is omitted for simplicity. This ionization rate is similar to the commonly used ADK rate [32–34]

$$W_{\text{ADK}}(k_\perp, F) \approx \exp\left[-\frac{2(k_\perp^2 + 2I_p)^{3/2}}{3F}\right], \tag{14}$$

but with a different denominator in the exponent. Equation (13) has been derived in Ref. [31]. Here, we show that this simple modification improves the way nonadiabaticity is taken into account with respect to the ADK theory significantly. The field derivative $\boldsymbol{F}'$ in Eq. (13) introduces the dependence of the tunneling rate on the carrier frequency ω and the pulse envelope, and it is easy to infer that the nonadiabaticity induced by the envelope is smaller than that from the carrier. Along the same line, the exit position can be obtained from

$$\boldsymbol{r}_{\text{SFA-AE}}(\boldsymbol{k}_\perp, \boldsymbol{F}) = -\frac{\boldsymbol{F}}{2}\frac{k_\perp^2 + 2I_p}{F^2 - \boldsymbol{k}_\perp\cdot\boldsymbol{F}'}, \tag{15}$$

while the ADK theory gives

$$\boldsymbol{r}_{\text{ADK}}(k_\perp, \boldsymbol{F}) = -\frac{\boldsymbol{F}}{2}\frac{k_\perp^2 + 2I_p}{F^2}. \tag{16}$$

In Fig. 4(b), we show the tunneling exit characteristics obtained by the adiabatic expansion of the SFA. Obviously, the exit conditions are very close to those of the full SFA results in Fig. 4(a).

The result of the ADK theory is shown in Fig. 4(c), which replaces the denominator $\sqrt{F^2 - \boldsymbol{k}_\perp\cdot\boldsymbol{F}'}$ in the adiabatic expansion SFA by F. It gives a much narrower distribution of tunneling exit position [Fig. 4(c1)]. Note that the exit position is still a distribution instead of a line because of the transverse tunneling momentum $k_\perp$ at the exit (16). This effect can also be observed in the broadening of the distribution of exit points in the dynamic position criterion with respect to the static one, see Fig. 1(g1). If $k_\perp$ is set to 0, then the tunneling exit position reduces to a line $-\hat{\boldsymbol{F}}I_p/F$. The distribution of tunneling exit time [Fig. 4(c2)] is also slightly narrower due to neglect of nonadiabatic effects, which in addition results in a distribution of transverse tunneling momentum centered at zero [Fig. 4(c4)]. The complete neglect of nonadiabaticity is best illustrated in the electron energy at the tunnel exit [Fig. 4(c5)], which sits exactly at the ground-state energy $-I_p$.

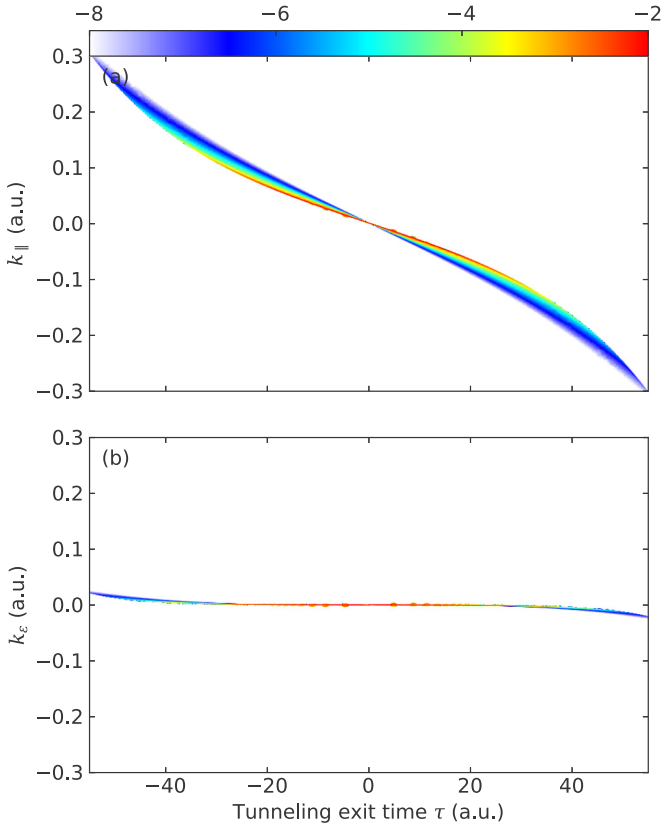

FIG. 5. Correlated distribution of tunneling exit time τ and (a) longitudinal tunneling momentum $k_\parallel$ and (b) elliptical tunneling momentum k_ε, for the model helium atom obtained by full SFA (in logarithmic scale). Laser parameters are the same as in Fig. 1.

This comes straight from

$$E_{\text{ADK}} = \tfrac{1}{2}k_\perp^2 + \boldsymbol{F}\cdot\boldsymbol{r}_{\text{ADK}} = -I_p. \tag{17}$$

Above comparison of the results from the adiabatic expansion of SFA and the ADK theory clearly shows that for the present case of circularly polarized laser fields, the slight modification in the denominator of the exponent in the tunneling ionization rate given in Eq. (13) incorporates nonadiabatic effects during tunneling ionization accurately.

As a matter of fact, the SFA calculations may even serve as a guide to deduce new improved velocity-based criteria. We show in Fig. 5(a) the correlated distribution of tunneling exit time τ and longitudinal tunneling momentum $k_\parallel$ from SFA. Although not big, clear deviation from zero is observed for $k_\parallel$. As discussed, $k_\parallel = 0$ results from a second-order adiabatic expansion of the saddle-point equation (5) in terms of small t_i. Indeed, one can expand it to the third order, giving an improved velocity criterion

$$k_\varepsilon \equiv -\boldsymbol{k}\cdot\hat{\boldsymbol{F}} - \frac{3\boldsymbol{F}\cdot\boldsymbol{F}' - \boldsymbol{k}\cdot\boldsymbol{F}''}{6F}\frac{k^2 + 2I_p}{F^2 - \boldsymbol{k}\cdot\boldsymbol{F}'} = 0. \tag{18}$$

For a circularly polarized long pulse, this criterion reduces to the velocity criterion (3a) [57]. We name this criterion the "elliptical velocity criterion," since its improvement could become noticeable when a short and/or elliptically polarized laser pulse is used. We show the correlated distribution of τ

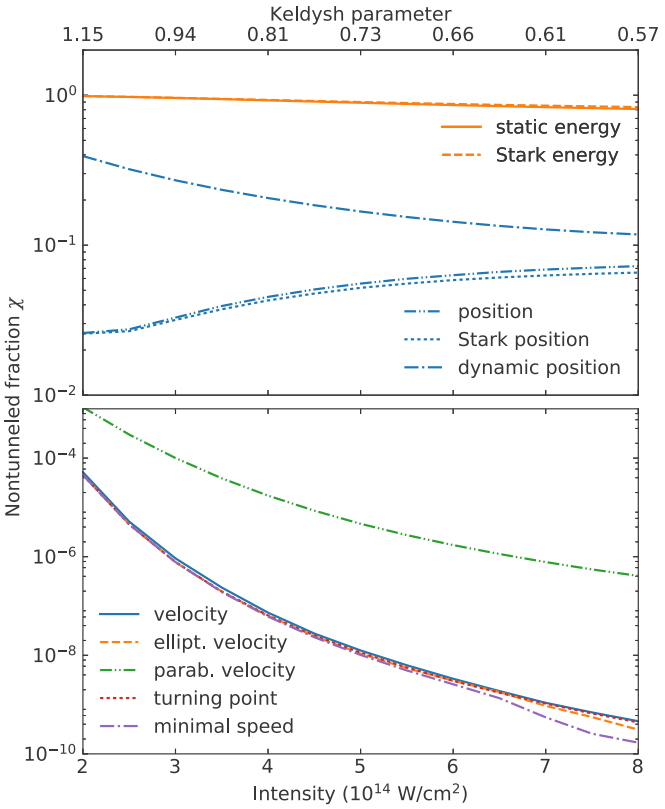

FIG. 6. Nontunneled fraction χ given by different tunneling criteria during the backpropagation of the ionized wave packet of the model helium atom. Laser parameters are the same as in Fig. 1 except for a varying peak intensity.

and k_ε from SFA calculations in Fig. 5(b), where k_ε is much more concentrated to zero than $k_\parallel$.

We then apply the elliptical velocity criterion to the classical backpropagation and show the results in Fig. 4(d), which are similar to those from the velocity criterion but with a longitudinal tunneling momentum closer to SFA results in Fig. 4(a).

As an extension to the current work, it would be interesting to study the exit characteristics in the case of elliptically or linearly polarized pulses, where the elliptical velocity criterion is expected to provide more improvements to the velocity criterion using classical backpropagation.

V. APPLICABILITY OF DIFFERENT TUNNELING CRITERIA

We now study the intensity dependence of the nontunneled fraction given by different tunneling criteria in Fig. 6. For the parameters chosen here, ionization takes place mostly in the tunneling regime, as can be seen from the Keldysh parameter in Fig. 6. It is clear that velocity-based criteria (velocity, elliptical velocity, parabolic velocity, turning point, and minimal speed criteria) result in a very low nontunneled fraction, which means that the majority of the ionization probability is accounted for under the corresponding mechanism. Moreover, the changing trend of the nontunneled fraction from adiabatic to nonadiabatic tunneling ionization is in agreement with the tunneling picture: as the Keldysh parameter decreases, the ionization moves deeper into the tunneling regime and the nontunneled fraction decreases. In contrast, other tunneling criteria give quite high nontunneled fractions, with questionable trends. This means they are less suitable, or even invalid classical pictures of the tunneling process.

TABLE II. Applicability of different tunneling criteria.

Tunneling criterion	Nonadiabaticity	Consistency	Low χ
Velocity	✓	✓	✓
Elliptical velocity	✓	✓	✓
Parabolic velocity	✓	✓	✓
Turning point	✓	✓	✓
Minimal speed	✓	✓	✓
Position	Partial		
Stark position	Partial		
Dynamic position	Partial	✓	
Static energy		✓	
Stark energy		✓	

In Table II we summarize the applicability of different tunneling criteria as a classical description of the quantum tunneling dynamics. Here, three conditions are used:

(1) Whether the tunneling criterion includes nonadiabatic tunneling effects.

(2) Whether the tunneling criterion is self-consistent. As above, the (Stark) position criterion is inconsistent to the underlying static (Stark-shifted) tunneling energy assumption.

(3) Whether the tunneling criterion leads to a low nontunneled fraction χ in the known tunneling regime.

From this comparison, it is clear that only velocity-based criteria are suitable candidates as the classical picture of quantum tunneling. Also, they show zero tunneling time delay, in agreement with our conclusion before [16,17].

VI. CONCLUSION

We studied the tunneling ionization of a model helium atom in an intense, short, circularly polarized laser field with the classical backpropagation method and retrieved the initial tunneling exit information by propagating the ionized wave packet backward in time. Stopping the backpropagation in different ways, we studied and compared ten different tunneling criteria on the same footing. We showed that the previously studied velocity criterion (I) and the elliptical velocity (II), parabolic velocity (III), turning point (IV), and minimal speed criteria (V) proposed here are successful candidates. They are all rooted in the zero-kinetic-energy principle as the commonly accepted classical picture of the quantum tunneling dynamics. These velocity-based criteria fully and consistently incorporate nonadiabatic tunneling effects, they give intuitive tunneling exit coordinates, and are able to account for the observed tunneling ionization probability. Under these five criteria, a zero tunneling time delay is found. Position-based criteria have the same origin, but in addition assume static total tunneling energy, leading to inconsistencies and reduced capability to cover the observed ionization yield (high nontunneled fraction).

Positive tunneling time delays found using these criteria can thus be considered as a misinterpretation of the attoclock experimental data based on models that do not take full and consistent account for nonadiabaticity. Additionally, energy-based tunneling criteria fail completely.

In addition, the connection between the velocity criterion and SFA is explored and a set of simple ADK-like formulas [Eqs. (13) and (15)] is obtained to describe the tunneling exit characteristics. A nonadiabatic term is identified in the formula that accounts for the nonadiabaticity in a tunneling process accurately. As a step further, a third-order expansion of the saddle-point equation was utilized to propose the elliptical velocity criterion, under which the tunneling exit characteristics obtained through classical backpropagation agree well with those calculated using SFA. In particular, a narrow distribution of the longitudinal tunneling momentum $k_\parallel$ is reproduced nicely. We hope this article serves as a guide to future theoretical and experimental works, given that the characteristics provided here may well act as a precise set of initial conditions to launch classical trajectories in Monte Carlo–like simulations.

ACKNOWLEDGMENTS

We would like to thank M. Lein and S. V. Popruzhenko for helpful discussions. H.N. was supported by the Alexander von Humboldt-Stiftung. N.E. and F.O. acknowledge support from the Deutsche Forschungsgemeinschaft in the framework of the Priority Program "Quantum Dynamics in Tailored Intense Fields" (QUTIF, SPP 1840). C.R. acknowledges support from the MINECO project FIS2016-75652-P. N.I.S.-S. was supported by the Deutsche Forschungsgemeinschaft (Grant No. SH 1145/1-1).

APPENDIX: VARIANTS OF THE POSITION CRITERION

The position criterion (3e) studied here results from a number of approximations. Here we show that these approximations do not change the conclusion made.

In parabolic coordinates, the exit point in the tunneling coordinate $\eta = r - \hat{\boldsymbol{F}} \cdot \boldsymbol{r}$ is obtained from [38]

$$-\frac{\beta}{2\eta} + \frac{m^2-1}{8\eta^2} - \frac{F\eta}{8} = -\frac{I_p}{4}, \tag{A1}$$

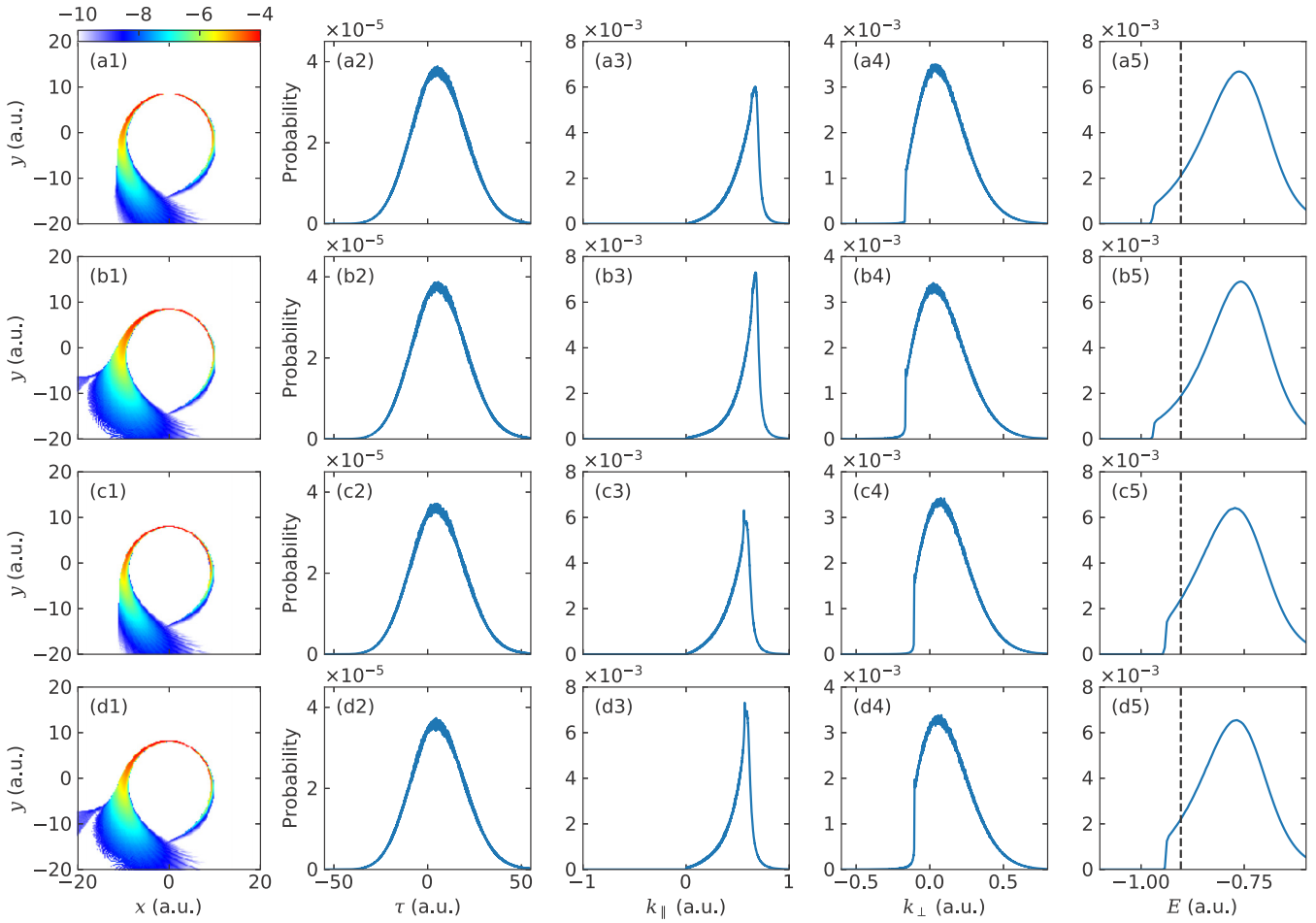

FIG. 7. Tunneling exit characteristics of the model helium atom obtained by variants of the position criterion. By row: (a) position criterion (3e); (b) full position criterion (A1); (c) two-dimensional position criterion (A6); (d) full two-dimensional position criterion (A4). By column: (1) distribution of tunneling exit position in x-y plane (in logarithmic scale); (2) distribution of tunneling exit time τ; (3) distribution of longitudinal tunneling momentum $k_\parallel$; (4) distribution of transverse tunneling momentum $k_\perp$; (5) distribution of tunneling energy E, where black dashed lines denote the ground-state energy $-I_p$. Laser parameters are the same as in Fig. 1.

where

$$\beta = Z - (|m|+1)\frac{\sqrt{2I_p}}{2} \tag{A2}$$

is the separation constant [38], Z is the charge of the parent ion, and m is the magnetic quantum number of the initial state. For typical laser parameters, $\eta \gg 1$, the $1/\eta^2$ term can be neglected in Eq. (A1), resulting in the solution

$$\eta = \frac{I_p + \sqrt{I_p^2 - 4\beta F}}{F}. \tag{A3}$$

Further assuming $-\boldsymbol{F} \parallel \boldsymbol{r}$, we have the position criterion (3e) [39]

$$r = \frac{I_p + \sqrt{I_p^2 - 4\beta F}}{2F}. \tag{3e}$$

Figure 7(a) shows the tunneling exit characteristic obtained from the position criterion (3e), which is a replica of Fig. 1(e). Figure 7(b) shows the corresponding tunneling exit information obtained from the full position criterion (A1). Obviously, the results are similar and the same problems persist for the full position criterion.

The full two-dimensional exit point can be obtained from the three-dimensional version (A1) by simply replacing $|m|$ with $|m| - \frac{1}{2}$:

$$-\frac{\beta_{2D}}{2\eta_{2D}} + \frac{\left(|m| - \frac{1}{2}\right)^2 - 1}{8\eta_{2D}^2} - \frac{F\eta_{2D}}{8} = -\frac{I_p}{4}, \tag{A4}$$

where

$$\beta_{2D} = Z - \left(|m| + \frac{1}{2}\right)\frac{\sqrt{2I_p}}{2}. \tag{A5}$$

Further simplification results in the two-dimensional position criterion

$$r_{2D} = \frac{I_p + \sqrt{I_p^2 - 4\beta_{2D}F}}{2F}. \tag{A6}$$

Tunneling exit conditions from the 2D position criterion (A6) and the full 2D position criterion (A4) are shown in Figs. 7(c) and 7(d), respectively. Evidently, the results are once again similar and the conclusions made for the position criterion (3e) still hold.

We skip the Stark-shifted and dynamic versions of all these variants of the position criterion as they result in the same conclusions. We stress that the problems encountered with the position-based criteria arise because they do not fully and consistently include the nonadiabaticity. Therefore, velocity-based criteria should be used in the nonadiabatic process of tunneling ionization.

[1] J. L. Krause, K. J. Schafer, and K. C. Kulander, Phys. Rev. Lett. **68**, 3535 (1992).
[2] J. J. Macklin, J. D. Kmetec, and C. L. Gordon, Phys. Rev. Lett. **70**, 766 (1993).
[3] T. Popmintchev, M.-C. Chen, P. Arpin, M. M. Murnane, and H. C. Kapteyn, Nat. Photon. **4**, 822 (2010).
[4] L. A. MacColl, Phys. Rev. **40**, 621 (1932).
[5] R. Landauer and T. Martin, Rev. Mod. Phys. **66**, 217 (1994).
[6] A. S. Landsman and U. Keller, Phys. Rep. **547**, 1 (2015).
[7] C. M. Maharjan, A. S. Alnaser, X. M. Tong, B. Ulrich, P. Ranitovic, S. Ghimire, Z. Chang, I. V. Litvinyuk, and C. L. Cocke, Phys. Rev. A **72**, 041403(R) (2005).
[8] P. Eckle, M. Smolarski, P. Schlup, J. Biegert, A. Staudte, M. Schöffler, H. G. Muller, R. Dörner, and U. Keller, Nat. Phys. **4**, 565 (2008).
[9] T.-M. Yan and D. Bauer, Phys. Rev. A **86**, 053403 (2012).
[10] M. Klaiber, K. Z. Hatsagortsyan, and C. H. Keitel, Phys. Rev. Lett. **114**, 083001 (2015).
[11] Th. Keil, S. V. Popruzhenko, and D. Bauer, Phys. Rev. Lett. **117**, 243003 (2016).
[12] P. Eckle, A. N. Pfeiffer, C. Cirelli, A. Staudte, R. Dörner, H. G. Muller, M. Büttiker, and U. Keller, Science **322**, 1525 (2008).
[13] M. Li, J. W. Geng, H. Liu, Y. Deng, C. Wu, L. Y. Peng, Q. Gong, and Y. Liu, Phys. Rev. Lett. **112**, 113002 (2014).
[14] X. Song, C. Lin, Z. Sheng, P. Liu, Z. Chen, W. Yang, S. Hu, C. D. Lin, and J. Chen, Sci. Rep. **6**, 28392 (2016).
[15] N. I. Shvetsov-Shilovski, M. Lein, L. B. Madsen, E. Räsänen, C. Lemell, J. Burgdörfer, D. G. Arbó, and K. Tőkési, Phys. Rev. A **94**, 013415 (2016).
[16] H. Ni, U. Saalmann, and J. M. Rost, Phys. Rev. Lett. **117**, 023002 (2016).
[17] H. Ni, U. Saalmann, and J. M. Rost, Phys. Rev. A **97**, 013426 (2018).
[18] B. Feuerstein and U. Thumm, J. Phys. B **36**, 707 (2003).
[19] X. Wang, J. Tian, and J. H. Eberly, Phys. Rev. Lett. **110**, 243001 (2013).
[20] X. Wang, J. Tian, and J. H. Eberly, J. Phys. B **51**, 084002 (2018).
[21] A. N. Pfeiffer, C. Cirelli, M. Smolarski, D. Dimitrovski, M. Abu-samha, L. B. Madsen, and U. Keller, Nat. Phys. **8**, 76 (2012).
[22] A. S. Landsman, M. Weger, J. Maurer, R. Boge, A. Ludwig, S. Heuser, C. Cirelli, L. Gallmann, and U. Keller, Optica **1**, 343 (2014).
[23] L. Torlina, F. Morales, J. Kaushal, I. A. Ivanov, A. Kheifets, A. Zielinski, A. Scrinzi, H. G. Muller, S. Sukiasyan, M. Y. Ivanov, and O. Smirnova, Nat. Phys. **11**, 503 (2015).
[24] N. Teeny, E. Yakaboylu, H. Bauke, and C. H. Keitel, Phys. Rev. Lett. **116**, 063003 (2016).
[25] N. Camus, E. Yakaboylu, L. Fechner, M. Klaiber, M. Laux, Y. Mi, K. Z. Hatsagortsyan, T. Pfeifer, C. H. Keitel, and R. Moshammer, Phys. Rev. Lett. **119**, 023201 (2017).
[26] U. S. Sainadh, H. Xu, X. Wang, Atia-Tul-Noor, W. X. Wallace, N. Douguet, A. W. Bray, I. A. Ivanov, K. Bartschat, A. S. Kheifets, R. T. Sang, and I. V. Litvinyuk, arXiv:1707.05445.
[27] N. Eicke and M. Lein, Phys. Rev. A **97**, 031402(R) (2018).
[28] S. P. Goreslavski and S. V. Popruzhenko, Sov. Phys. JETP **83**, 661 (1996).
[29] N. I. Shvetsov-Shilovski, S. V. Popruzhenko, and S. P. Goreslavski, Laser Phys. **13**, 1054 (2003).
[30] S. P. Goreslavski, G. G. Paulus, S. V. Popruzhenko, and N. I. Shvetsov-Shilovski, Phys. Rev. Lett. **93**, 233002 (2004).
[31] M. V. Frolov, N. L. Manakov, A. A. Minina, S. V. Popruzhenko, and A. F. Starace, Phys. Rev. A **96**, 023406 (2017).

[32] M. V. Ammosov, N. B. Delone, and V. P. Krainov, Sov. Phys. JETP **64**, 1191 (1986).
[33] N. B. Delone and V. P. Krainov, Phys. Usp. **41**, 469 (1998).
[34] M. Y. Ivanov, M. Spanner, and O. Smirnova, J. Mod. Opt. **52**, 165 (2005).
[35] X. M. Tong and C. D. Lin, J. Phys. B **38**, 2593 (2005).
[36] L. V. Keldysh, Sov. Phys. JETP **20**, 1307 (1965).
[37] S. V. Popruzhenko, J. Phys. B **47**, 204001 (2014).
[38] C. Z. Bisgaard and L. B. Madsen, Am. J. Phys. **72**, 249 (2004).
[39] C. Hofmann, A. S. Landsman, C. Cirelli, A. N. Pfeifer, and U. Keller, J. Phys. B **46**, 125601 (2013).
[40] J. W. Geng, L. Qin, M. Li, W. H. Xiong, Y. Liu, Q. Gong, and L. Y. Peng, J. Phys. B **47**, 204027 (2014).
[41] J. W. Geng, W. H. Xiong, X. R. Xiao, L. Y. Peng, and Q. Gong, Phys. Rev. Lett. **115**, 193001 (2015).
[42] C. Hofmann, T. Zimmermann, A. Zielinski, and A. S. Landsman, New J. Phys. **18**, 043011 (2016).
[43] J. Tian, X. Wang, and J. H. Eberly, Phys. Rev. Lett. **118**, 213201 (2017).
[44] J. Cai, Y. J. Chen, Q. Z. Xia, D. F. Ye, J. Liu, and L. B. Fu, Phys. Rev. A **96**, 033413 (2017).
[45] A. M. Perelomov, V. S. Popov, and M. V. Terent'ev, Sov. Phys. JETP **23**, 924 (1966).
[46] A. M. Perelomov, V. S. Popov, and M. V. Terent'ev, Sov. Phys. JETP **24**, 207 (1967).
[47] A. M. Perelomov and V. S. Popov, Sov. Phys. JETP **25**, 336 (1967).
[48] V. D. Mur, S. V. Popruzhenko, and V. S. Popov, J. Exp. Theor. Phys. **92**, 777 (2001).
[49] V. S. Popov, Phys. Usp. **47**, 855 (2004).
[50] B. M. Karnakov, V. D. Mur, S. V. Popruzhenko, and V. S. Popov, Phys. Usp. **58**, 3 (2015).
[51] M. Klaiber and J. S. Briggs, Phys. Rev. A **94**, 053405 (2016).
[52] G. F. Gribakin and M. Y. Kuchiev, Phys. Rev. A **55**, 3760 (1997).
[53] T. K. Kjeldsen and L. B. Madsen, Phys. Rev. A **74**, 023407 (2006).
[54] D. B. Milošević, G. G. Paulus, D. Bauer, and W. Becker, J. Phys. B **39**, R203 (2006).
[55] M. Li, J. W. Geng, M. Han, M. M. Liu, L. Y. Peng, Q. Gong, and Y. Liu, Phys. Rev. A **93**, 013402 (2016).
[56] M. Li, M.-M. Liu, J.-W. Geng, M. Han, X. Sun, Y. Shao, Y. Deng, C. Wu, L.-Y. Peng, Q. Gong, and Y. Liu, Phys. Rev. A **95**, 053425 (2017).
[57] In this case, $\hat{\boldsymbol{F}} \perp \boldsymbol{F}'$ and $\hat{\boldsymbol{F}} \parallel \boldsymbol{F}''$, the elliptical velocity criterion, becomes $k_\varepsilon = -(1 + \frac{\omega^2}{6}\frac{k^2+2I_p}{F^2-\boldsymbol{k}\cdot\boldsymbol{F}'})\boldsymbol{k}\cdot\hat{\boldsymbol{F}} = 0$. This is equivalent to $k_\parallel = -\boldsymbol{k}\cdot\hat{\boldsymbol{F}} = 0$, the velocity criterion.